Journal of Power Sources 245 (2014) 787–795

Contents lists available at SciVerse ScienceDirect

Journal of Power Sources

journal homepage: www.elsevier.com/locate/jpowsour

Creep rupture of the joint of a solid oxide fuel cell glass–ceramic sealant with metallic interconnect

Chih-Kuang Lin [a,*], Kun-Liang Lin [a], Jing-Hong Yeh [a], Si-Han Wu [b], Ruey-Yi Lee [b]

[a] Department of Mechanical Engineering, National Central University, Jhong-Li 32001, Taiwan
[b] Physics Division, Institute of Nuclear Energy Research, Lung-Tan 32546, Taiwan

HIGHLIGHTS

- Creep strength of SOFC glass seal/metal interconnect joint is assessed at 800 °C.
- Creep life time increases with a decrease in both tensile and shear loads applied.
- Prolonged constant tensile load degrades joint strength more than shear load.
- Creep fracture patterns of both shear and tensile joint specimens are similar.
- Creep crack growth occurs mostly along and around the chromate/glass interface.

ARTICLE INFO

Article history:
Received 1 May 2013
Received in revised form
8 July 2013
Accepted 9 July 2013
Available online 17 July 2013

Keywords:
Planar solid oxide fuel cell
Glass–ceramic sealant
Metallic interconnect
Creep
Joint strength

ABSTRACT

Creep properties of sandwich joint specimens made of a newly developed $BaO–B_2O_3–Al_2O_3–SiO_2$ glass–ceramic sealant (GC-9) and a ferritic-stainless-steel interconnect (Crofer 22 H) for planar solid oxide fuel cells (pSOFCs) are investigated at 800 °C under constant shear and tensile loadings. The creep rupture time of Crofer 22 H/GC-9/Crofer 22 H joint specimens is increased with a decrease in applied load for both shear and tensile loading modes. The given metal/sealant/metal joint has a greater degradation of joint strength at 800 °C under prolonged, constant tensile loading as compared to shear loading. The tensile creep strength at a rupture time of 1000 h is about 9% of the average tensile joint strength, while the shear creep strength at 1000 h is about 23% of the average shear joint strength. Failure patterns of both shear and tensile joint specimens are similar regardless of the creep rupture time. In general, creep cracks initiate at the interface between the $(Cr,Mn)_3O_4$ spinel layer and the $BaCrO_4$ chromate layer, penetrate through the $BaCrO_4$ layer, and propagate along the interface between the chromate layer and glass–ceramic substrate until final fracture. Final, fast fracture occasionally takes place within the glass–ceramic layer.

1. Introduction

In recent development of solid oxide fuel cell (SOFC), planar SOFCs (pSOFCs) attract more attention than tubular ones as they are cost effective and have a lower Ohmic loss [1]. A pSOFC stack is generally a multi-layer structure composed of repeated units of ceramic anode–electrolyte–cathode assembly and metallic components. In particular, interconnects play a very important role in structural and electrical connection of unit cells. To maintain the operation and performance of a pSOFC system, hermetic sealants are needed to bond components and form gas-tight seals to separate both the oxidant and fuel chambers. When a rigid type of sealing is applied to pSOFC stacks, joining glass–ceramic sealants to metallic interconnects is very common. Locations of sealant applied in a pSOFC stack include: (a) cell to metal frame; (b) metal frame to metal interconnect; (c) frame/interconnect pair to electrically insulating spacer; (d) stack to base manifold plate [2]. Seals at locations (b) and (d) can be regarded as a joint of glass–ceramic sealant and metallic interconnect.

The high-temperature operation of SOFC could generate significant thermal stresses due to mismatch of coefficient of thermal expansion (CTE) between components and temperature gradients in the SOFC system [3–5]. Detailed configuration of the joint between glass–ceramic sealant and metallic interconnect in real pSOFC stacks is given in Refs. [2–4] to illustrate how and where thermal stresses are generated in such a joint. The thermal stresses

* Corresponding author. Tel.: +886 3 426 7340; fax: +886 3 425 4501.
E-mail address: t330014@cc.ncu.edu.tw (C.-K. Lin).

0378-7753/$ – see front matter © 2013 Elsevier B.V. All rights reserved.
http://dx.doi.org/10.1016/j.jpowsour.2013.07.047

may or may not cause an immediate failure of pSOFC structure, but they could generate creep damages in the components under a long-term high-temperature operation environment. Creep damages in the joint of a glass–ceramic sealant with metallic interconnect may eventually generate excessive deformation and/or cracking, leading to gas leakage and degradation of cell performance. Therefore, it is very important to investigate the creep properties of such a joint for assessing the structural integrity and durability of a pSOFC stack.

The high-temperature creep properties have been studied individually for glass–ceramic sealants [6–9] and metallic interconnects [10–13] for pSOFC applications. However, the mechanical properties of a joint do not belong to that of a single material while they are interfacial properties between two materials. Any interaction between the glass–ceramic sealant and metallic interconnect may influence the mechanical properties of the joint. Although a few studies have investigated the mechanical properties of the joint of SOFC glass–ceramic sealant/metallic interconnect [6,14–19], there is still lack of study on the long-term high-temperature creep behavior of such a joint. As a reliable pSOFC system is expected to operate steadily at elevated temperature for a prolonged period of time (at least 20,000 h for commercial systems), more studies are needed to investigate the creep behavior of joints between the glass–ceramic sealant and interconnect at high-temperature. As part of a series of studies [9–11,19–23] on the mechanical properties of glass–ceramic sealants and metallic interconnects for pSOFCs, the aim of this study is to investigate the high-temperature creep rupture behavior of the joint between a newly developed $BaO–B_2O_3–Al_2O_3–SiO_2$ glass–ceramic sealant (GC-9) and a ferritic-stainless-steel interconnect (Crofer 22 H) under both tensile and shear loadings.

2. Experimental procedures

2.1. Materials and specimens

As described above, glass–ceramic sealants bonding a metallic frame to a metallic interconnect and a stack to a base manifold plate are classified as a joint of glass–ceramic sealant and metallic interconnect. In order to simulate such a joint subjected to thermal stresses at operating temperature, two types of sandwich joint specimens (metal/sealant/metal) are applied to determine the tensile and shear creep properties of the joint. In consideration of interfacial fracture in a joint of two dissimilar materials, failure often occurs along the interface such that compressive loads normal to the interface are not expected to generate interfacial cracking or debonding along the interface. Therefore, only tensile and shear loadings are applied to the joint specimens for creep test in the current study. Details of the specimen geometry and dimensions are given in a previous study [19]. The metallic coupons of the joint specimens are made of a newly developed commercial ferritic stainless steel, Crofer 22 H (ThyssenKrupp VDM GmbH, Germany), for pSOFC interconnects. Chemical composition of Crofer 22 H alloy in wt% includes 22.93 Cr, 1.94 W, 0.51 Nb, 0.43 Mn, 0.21 Si, 0.08 La, 0.07 Ti, 0.02 Cu, 0.02 Al, 0.014 P, 0.007 C, <0.002 S, and balance of Fe. Relevant mechanical properties of Crofer 22 H alloy can be found in a previous study [11]. In order to minimize bending and twisting effects during creep testing, the force is applied to the joint specimen by means of pin loading. The as-received, 2.5-mm-thick metal plates were cut into rectangular slices with dimensions of 95 mm (length) × 25 mm (width) × 2.5 mm (thickness). A pin hole was drilled in each steel slice. For shear test specimens, one edge of each steel slice was milled from the original thickness of 2.5 mm to 1 mm with an area of 8 mm × 25 mm to be spread with the glass–ceramic sealant. The nominal joining areas are 25 mm × 2.5 mm and 25 mm × 6 mm for tensile and shear test specimens, respectively.

In each joint specimen, a novel $BaO–B_2O_3–Al_2O_3–SiO_2$ glass–ceramic sealant (designated as GC-9), which was developed at the Institute of Nuclear Energy Research for pSOFC sealing, is applied to join the two metallic coupons. Chemical composition of the patent GC-9 glass–ceramic in mol% includes 34 BaO, 9.5 B_2O_3, 4.5 Al_2O_3, 34 SiO_2, 12 CaO, 5 La_2O_3, and 1 ZrO_2 [24]. Relevant material properties of GC-9 glass–ceramic have been reported previously [9,20–22,25–29]. After machining the steel slices, GC-9 glass paste was spread on the joining region of each steel coupon to make a half specimen. A joint specimen was assembled by placing a half specimen on another half specimen to form a metal/glass–ceramic/metal sandwich specimen through appropriate heat treatments. After the joining process was completed, the thickness of glass–ceramic sealant is of 0.5 mm for the shear test specimen and of 0.44 mm for the tensile test specimen. As the joint specimens were prepared and fabricated in a way similar to that of a previous study, details of materials and specimen preparation can be found in that study [19].

2.2. Creep test

Tensile and shear creep tests were conducted at 800 °C under a constant load using a direct-load creep test machine. Various weights were used as the loading source in the direct-load creep test machine. The stress level can be adjusted by changing the weights applied. For tensile creep tests, various constant loads of 180 N–280 N were applied, while constant loads of 60 N–100 N were applied for the shear creep tests. The values of the applied constant loads were selected to generate the magnitude of creep rupture time distributed in the orders of 10^0, 10^1, 10^2, and 10^3 h. In each test, the joint specimen was heated to 800 °C with a rate of 5 °C min^{-1} and held for 15 min to reach thermal equilibrium before applying the mechanical load.

2.3. Microstructural analysis

After creep testing, fracture surfaces were examined with an optical microscope to determine the true joining area for calculating the nominal tensile or shear stress. Scanning electron microscopy (SEM) was employed to examine the failure mode as well as the interfacial morphology between the glass–ceramic sealant and metallic interconnect. The energy dispersive spectrometer (EDS) module attached with the SEM was used for composition analysis to show the elemental distributions in selected regions on the fracture surfaces.

3. Results and discussion

3.1. Creep rupture behavior

For the given joint specimens, the shear joint strength has an average value of 6.6 MPa and 4.7 MPa at room temperature and 800 °C, respectively, while the average tensile joint strength is of 23 MPa at room temperature and of 12.7 MPa at 800 °C [19]. Creep rupture characteristics of the Crofer 22 H/GC-9/Crofer 22 H joint subjected to constant shear and tensile loads at 800 °C are shown in Fig. 1 by plotting the applied stress versus creep rupture time. Four constant loads (280 N, 200 N, 190 N, and 180 N) are applied to the shear test specimens, corresponding to constant shear stresses of 1.04 MPa–1.60 MPa (Fig. 1(a)). For tensile test specimens, the applied constant loads are of 100 N, 80 N, 70 N, and 60 N, corresponding to constant tensile stresses of 0.96 MPa–1.60 MPa (Fig. 1(b)). As shown in Fig. 1, the relationship between the applied

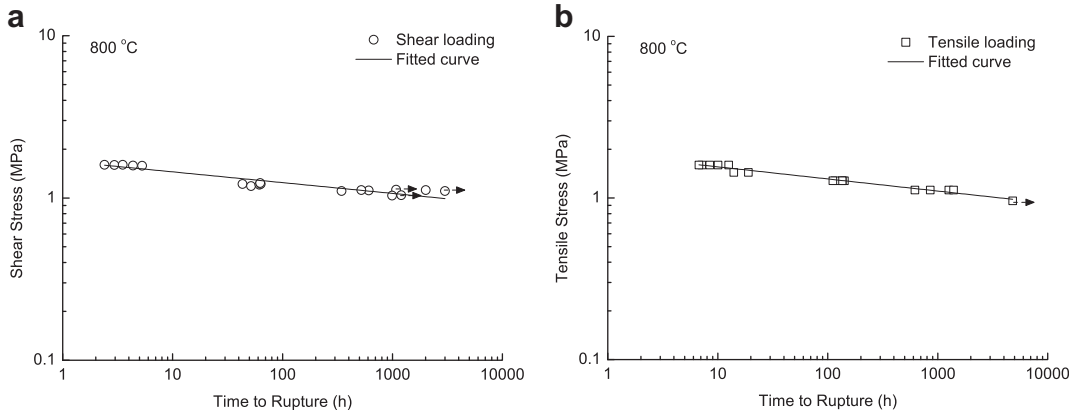

Fig. 1. Applied stress versus rupture time for the joint specimens subjected to constant (a) shear and (b) tensile loading. (Arrows indicate the specimens were not ruptured when the test was terminated.)

stress and creep rupture time is well described by a simple power–law for each loading mode. The fitted equation and correlation coefficient (r) for each loading mode in Fig. 1 are expressed as follows,

$$\text{shear loading}: \tau t_r^{0.066} = 1.68, \quad r^2 = 0.90 \tag{1}$$

$$\text{tensile loading}: \sigma t_r^{0.074} = 1.85, \quad r^2 = 0.97 \tag{2}$$

where τ and σ are the applied shear and tensile stresses in unit of MPa and t_r is time to rupture in unit of h. The creep rupture time of the joint subjected to a constant shear or tensile load at 800 °C can be estimated through these power–law relations thanks to the high correlation coefficient values.

As shown in Fig. 1, the creep rupture time increases with a decrease in applied stress for both loading modes. For an applied constant stress of about 1.6 MPa, the creep rupture time is less than 10 h for each loading mode. On the other hand, for a creep rupture time longer than 1000 h, the applied constant stress is smaller than 1.1 MPa for both loading modes. This applied shear stress level for a rupture time of 1000 h is about 23% of the average shear joint strength (4.7 MPa) at 800 °C. The tensile creep strength at 1000 h is only about 9% of the average tensile joint strength (12.7 MPa) at 800 °C. Apparently, the given metal/sealant/metal joint has a greater degradation of joint strength at 800 °C under prolonged, constant tensile loading as compared to shear loading. In other words, the creep resistance of the given joint at 800 °C, relative to its ultimate joint strength, is smaller in tensile loading mode than in shear loading mode.

According to a relation between minimum creep strain rate and applied tensile stress, the creep mechanism of bulk Crofer 22 H alloy at 800 °C is found to involve a power–law dislocation creep mechanism interacting with an in-situ precipitation strengthening mechanism [11]. Similarly, the creep mechanism for as-sintered, bulk GC-9 glass–ceramic subjected to constant bi-axial flexural loading at 800 °C also involves a power–law dislocation creep mechanism, based on a relation between apparent minimum creep strain rate and applied stress [9]. The creep strain is not measured in the present study for the given joint specimens because creep fracture takes place at the interface of GC-9/Crofer 22 H rather than in the glass–ceramic layer or in the metal part. Therefore, no such relationship of minimum creep strain rate vs. applied stress is available to deduce the creep mechanism at 800 °C for the given joint specimens. However, in a similar power–law relationship between the applied tensile stress and creep rupture time given in Eq. (2), the stress exponent value for bulk Crofer 22 H is 0.13 or 0.37 depending on the applied stress level [11], while it is 0.14, 0.051, and 0.057 for non-aged, 100 h-aged, and 1000 h-aged bulk GC-9, respectively [19]. As shown in Eq. (2), the stress exponent is 0.074 for the joint of CC-9/Crofer 22 H and it is close to that for variously aged bulk GC-9 tested at 800 °C. Whether this implies the tensile creep fracture of the given joint specimen also involves a dislocation type of creep mechanism is uncertain at this moment. As no creep tests have been conducted individually for bulk Crofer 22 H and GC-9 under shear loading at 800 °C, no comparison can be made for the stress exponent value of the joint specimens subjected to constant shear loading.

3.2. Failure analysis

Formation of adhesive oxide layers is the main mechanism of interfacial joining between the glass–ceramic sealant and metallic interconnect [30]. The high-temperature joining mechanism of the GC-9 glass–ceramic sealant and Crofer 22 H alloy involves formation of three oxide layers, namely a Cr_2O_3 chromia layer on the surface of Crofer 22 H, a $BaCrO_4$ chromate layer on the surface of GC-9, and a $(Cr,Mn)_3O_4$ spinel layer in between [19]. Optical micrographs of the typical fracture surfaces in the crept, shear specimens are shown in Fig. 2. Note that fracture surfaces on both halves of each broken specimen are presented in Fig. 2 with a mirror symmetry. As shown in Fig. 2(a), for a short creep rupture time (<100 h), creep cracks initiate at the interface between the spinel layer and $BaCrO_4$ layer at the periphery of the joining area and propagate into the $BaCrO_4$ layer, followed by final, fast fracture at the inner glass–ceramic substrate. Identification of each layer shown in Fig. 2 is confirmed through SEM/EDS analysis. SEM micrographs of two outlined regions (Regions 1 and 2) without adhered glass–ceramic in the upper micrograph of Fig. 2(a) are shown in Fig. 3. Fig. 3(a) shows a microstructure of $(Cr,Mn)_3O_4$ spinel layer in the peripheral region (Region 1) of Fig. 2(a). The inner region (Region 2) of Fig. 2(a) is a $BaCrO_4$ chromate layer with some embedded spinels, as shown in Fig. 3(b). The counterpart of Region 1, which corresponds to a yellow region in the lower micrograph of Fig. 2(a), is found to be a chromate structure, as shown in Fig. 3(c). Accordingly, the peripheral yellow regions in the optical micrographs of Fig. 2 indicate a $BaCrO_4$ chromate layer on top of the GC-9 glass–ceramic substrate. Note the white areas in Fig. 2(a) are identified as the interior of the GC-9 glass–ceramic layer. Therefore, fracture of the crept, shear specimens with a short rupture time occurs through delamination of the interface of $(Cr,Mn)_3O_4/BaCrO_4$ in the peripheral area, followed by

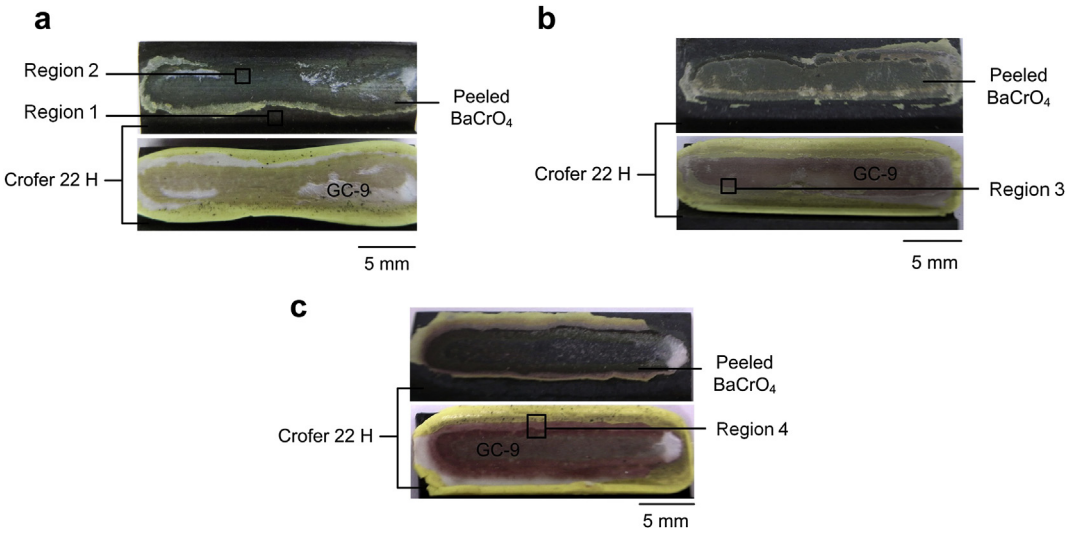

Fig. 2. Failure patterns in the shear joint specimens: (a) short creep rupture time; (b) medium creep rupture time; (c) long creep rupture time.

delamination of the interface of $BaCrO_4$/GC-9 and/or breaking within the glass–ceramic layer in the inner region.

For a medium creep rupture time (100 h $< t_r <$ 1000 h), cracking first takes place peripherally at the interface between the spinel layer and $BaCrO_4$ layer (yellow region in the lower micrograph of Fig. 2(b)), and then proceeds inward through the $BaCrO_4$ layer and along the interface between the chromate layer and glass–ceramic substrate (central pink region in the lower micrograph of Fig. 2(b)). The lime green film in the upper micrograph of Fig. 2(b) is a peeled $BaCrO_4$ layer on top of the Crofer 22 H side. SEM micrograph of an outlined region (Region 3) of the fracture surface with adhered glass–ceramic in the lower micrograph of Fig. 2(b) is shown in Fig. 4(a). As shown in Fig. 2(b), there are two distinct zones in Region 3, pink and light yellow. The pink zone contains some residual chromate on top of the GC-9 glass–ceramic and the light yellow zone is the chromate ($BaCrO_4$) layer. By means of EDS analysis, element distributions in these two zones are confirmed and shown in Fig. 4(b)–(f). A high intensity of Si and Al is found in the region of GC-9 glass–ceramic, as shown in Fig. 4(c) and (f). The region having a high intensity of Cr (Fig. 4(b)) and Ba

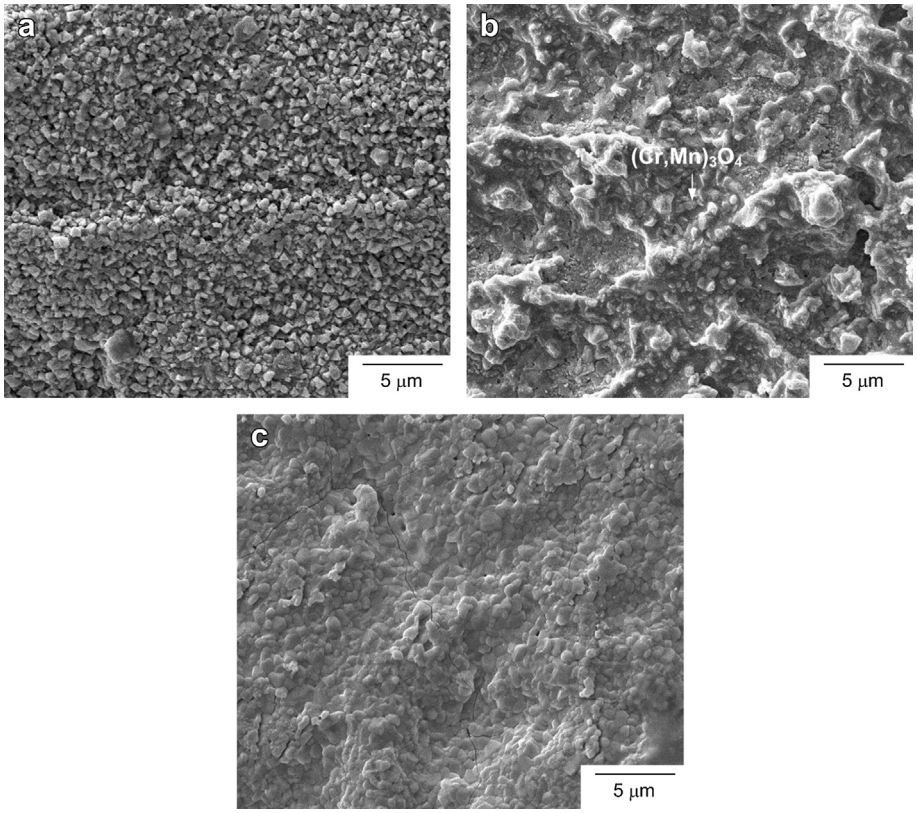

Fig. 3. SEM micrographs of selected regions in the shear joint specimen of Fig. 2(a): (a) Region 1; (b) Region 2; (c) counterpart of Region 1.

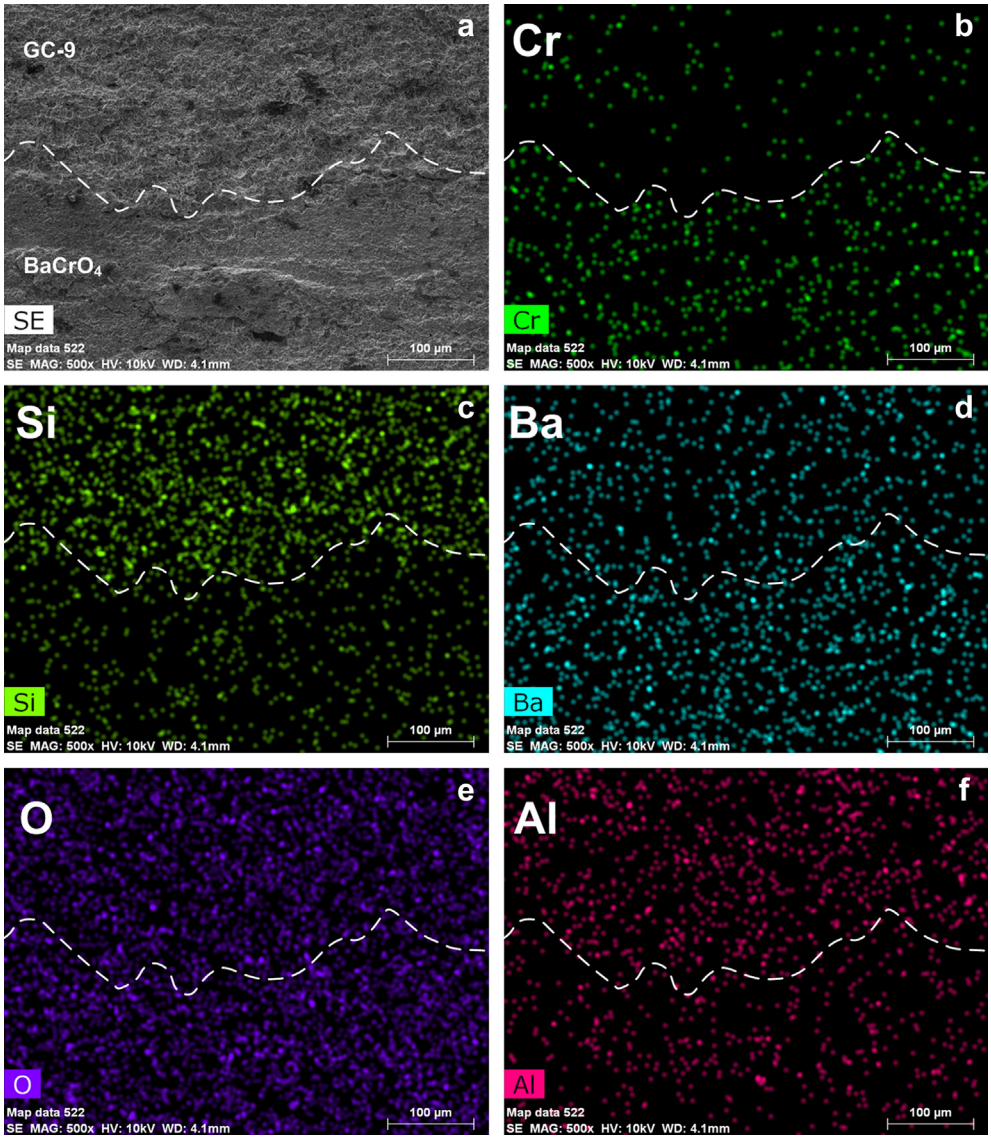

Fig. 4. EDS mapping of elements on Region 3 in the shear joint specimen of Fig. 2(b): (a) SEM micrograph of mapping region; (b) Cr; (c) Si; (d) Ba; (e) O; (f) Al.

(Fig. 4(d)) agrees with the corresponding $BaCrO_4$ layer. Therefore, the creep cracking path for shear specimens with a medium creep rupture time is generally similar to that of a short creep rupture time, as described above.

For a creep rupture time longer than 1000 h, four different colors (yellow, pink, red, and brown) are observed in the lower micrograph of Fig. 2(c). SEM micrograph of the outlined area (Region 4) in the lower micrograph of Fig. 2(c) is shown in Fig. 5. A linescan module of the SEM was applied to detect the major chemical elements in this area with various colors. Each sub-region in the observed area is labeled with the corresponding color, as shown in the SEM micrograph of Fig. 5. The arrow in Fig. 5 indicates the linescan direction is from bottom to top. The linescan results are shown in Fig. 6 by presenting the linescan arrow in a horizontal direction from left to right. A high intensity of Cr is found in the yellow region in comparison with the other regions, as shown in Fig. 6(f). It indicates again that the yellow region is a $BaCrO_4$ chromate layer on top of the GC-9 glass–ceramic substrate. The intensity of Al, Ca, and Si which are the compositions of GC-9 glass–ceramic is lower than that of Cr in this yellow region, as

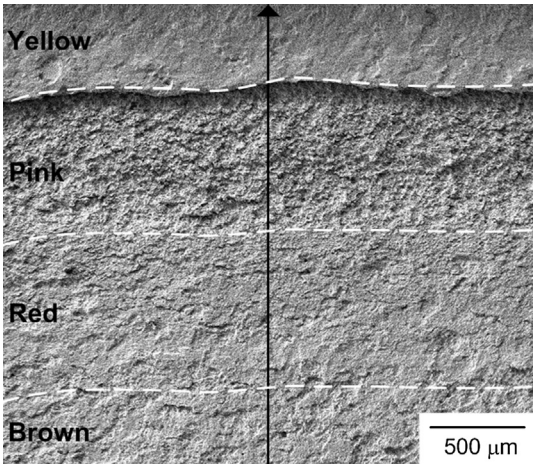

Fig. 5. SEM micrograph of Region 4 in the shear joint specimen of Fig. 2(c). (Arrow indicates the direction of linescan analysis.)

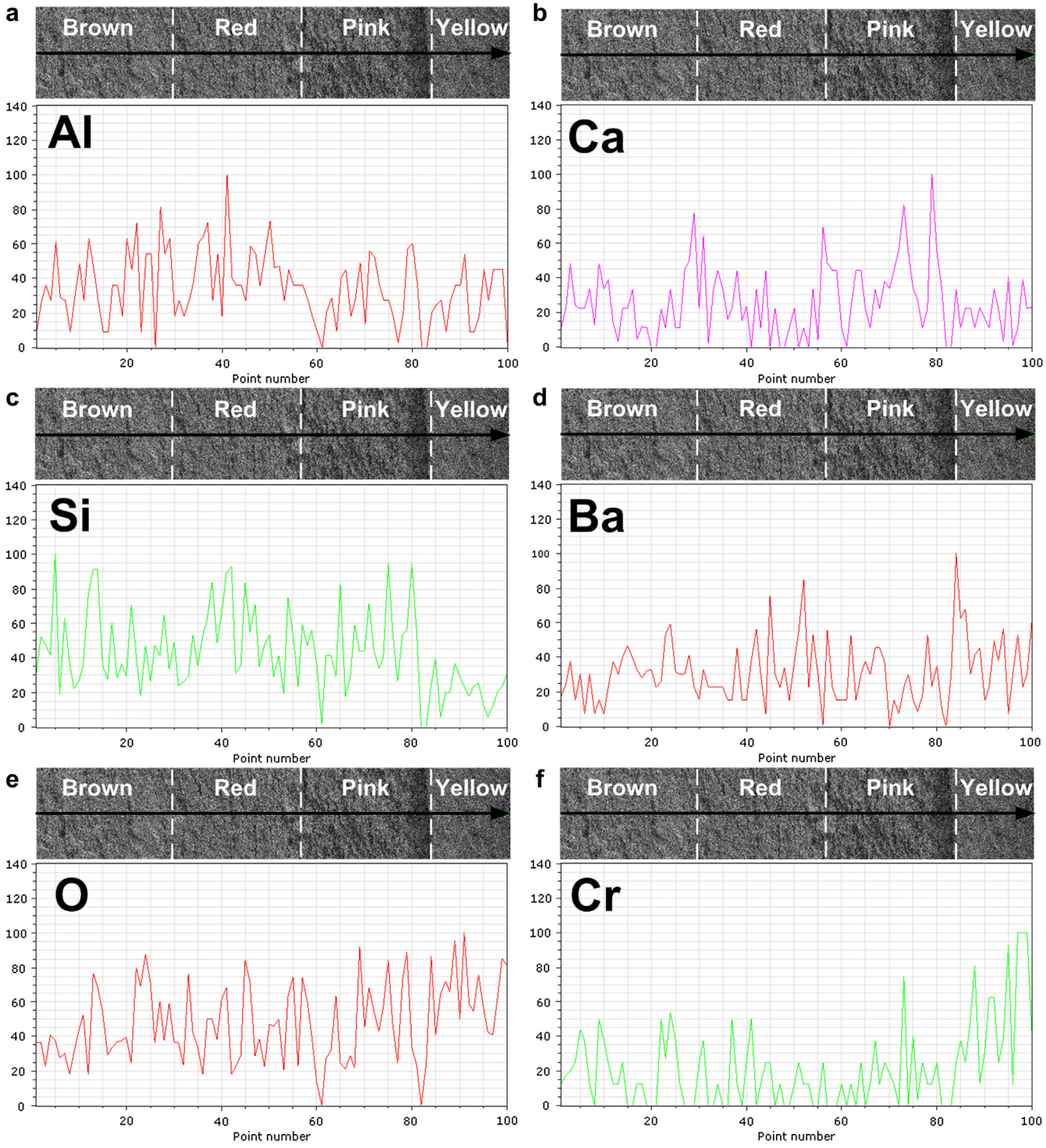

Fig. 6. Linescan analysis of element distribution in Fig. 5: (a) Al; (b) Ca; (c) Si; (d) Ba; (e) O; (f) Cr. (Direction of the arrow in the SEM micrograph is the same as that in Fig. 5.)

shown in Fig. 6. On the other hand, a high intensity of Al, Ca, and Si is observed in the pink, red, and brown regions in contrast to the yellow region (Fig. 6). In the upper micrograph of Fig. 2(c), some white glass–ceramic spots are left on top of the Crofer 22 H surface, corresponding to the pink, red, and brown regions in the lower micrograph of Fig. 2(c). The pink, red, and brown colors indicate that some chromate is left on top of the glass–ceramic substrate. A greater amount of leftover chromate is observed in the red and brown regions, as compared to the pink region. The yellow region which is the initial cracking area represents a weaker interface between the spinel layer and $BaCrO_4$ layer. The slow crack growth regions (pink, red, and brown) accompany a leftover chromate on the GC-9 substrate. Final fast fracture occasionally occurs within the white glass–ceramic substrate. Therefore, the crack propagating path in the shear specimens with a much longer creep rupture time (>1000 h) is similar to that with a medium creep rupture time, but with a deeper color in the slow crack growth region.

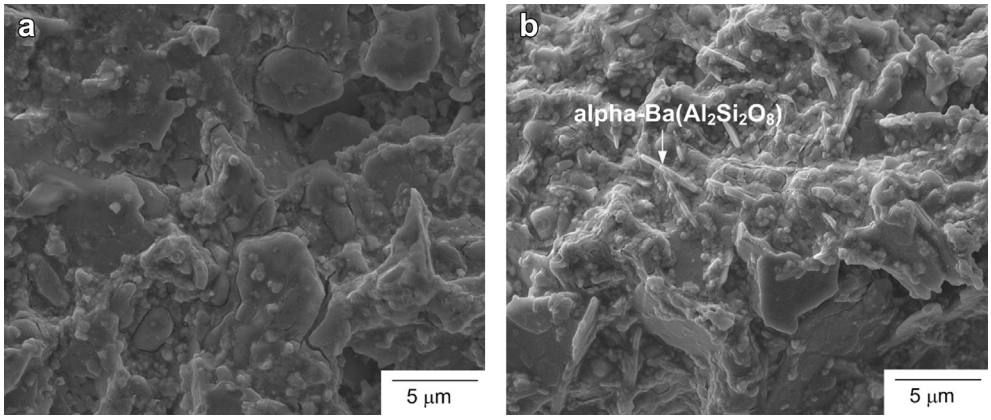

Fig. 7. Comparison of microstructure of GC-9 glass–ceramic substrate with residual chromate: (a) pink region in the lower part of Fig. 2(b); (b) brown region in the lower part of Fig. 2(c).

In the previous study of Lin et al. [19], the GC-9 glass–ceramic layer on the fracture surface in a 1000-h pre-aged joint specimen also shows a brown color. That joint specimen was aged first at 800 °C for 1000 h before undergoing a quick shear strength test at 800 °C. For non-aged or short-term pre-aged (250 h and 500 h) joint specimens, the GC-9 glass–ceramic layer on the fracture surface exhibits a white color after a quick shear strength test at 800 °C [19]. For a pure GC-9 glass–ceramic disk sample aged at 800 °C for 1000 h, no color change into red or brown is observed on the fracture surface after a quick bi-axial flexural strength test at 800 °C [9]. An exhibition of different colors on the fracture surface of a medium- or long-term crept specimen is attributed to the leftover $BaCrO_4$ chromate on the glass–ceramic substrate. When the chromate is left on the Crofer 22 H side, a lime green color is observed. When the chromate is left on the glass–ceramic substrate, pink, red, and brown colors are observed. Therefore, the leftover chromate is related to the change of glass–ceramic color in the slow crack growth area on the fracture surface of the crept, shear specimens.

Comparison of the GC-9 glass–ceramic microstructure for two different creep rupture times of shear specimens (Fig. 2(b) and (c)) is shown in Fig. 7. As shown in Fig. 7(b), more needle-shape crystalline phases (alpha-$Ba(Al_2Si_2O_8)$) are observed in the brown region of a long-term crept specimen, in comparison with the pink region of a medium-term crept specimen (Fig. 7(a)). Apparently, an in-situ crystallization mechanism takes place in the glass–ceramic and causes the glass–ceramic layer to have a greater brittleness in a long-term crept specimen. Therefore, the creep crack initiates at the weakest spinel/$BaCrO_4$ interface firstly, penetrates through the chromate layer, and propagates along the interface between the chromate layer and glass–ceramic substrate with brittle crystalline phases during a long-term creep test.

Typical fracture surfaces for crept, tensile specimens are shown in Fig. 8. Similar to the creep rupture under constant shear loading, creep cracks of tensile specimens initiate at the peripheral interface between the $BaCrO_4$ chromate layer and the $(Cr,Mn)_3O_4$ spinel layer. They subsequently penetrate through the chromate layer and propagate along the interface between the chromate layer and glass–ceramic substrate. Final fast fracture occasionally takes place within the glass–ceramic layer. Again, the central pink and red regions in the lower micrographs of Fig. 8(b) and (c) indicate some leftover chromate on the glass–ceramic substrate. Identification of each layer shown in Fig. 8 is also confirmed through SEM/EDS analysis in a way similar to that of crept, shear specimens. Take as an example the fracture surface for a medium creep rupture time ($100\ h < t_r < 1000\ h$) under tensile loading (Fig. 8(b)) to show the evidences. SEM micrographs of an outlined region (Region 5) without adhered glass–ceramic in the upper micrograph of Fig. 8(b) are shown in Fig. 9. Fig. 9(a) shows a high-magnification SEM micrograph of Region 5. SEM micrographs with a higher magnification for the microstructures of the spinel layer and glass–ceramic substrate in Fig. 9(a) are presented in Fig. 9(b) and (c), respectively. Crystalline phases are found in Fig. 9(c) for the glass–ceramic layer. It implies that the glass–ceramic substrate becomes

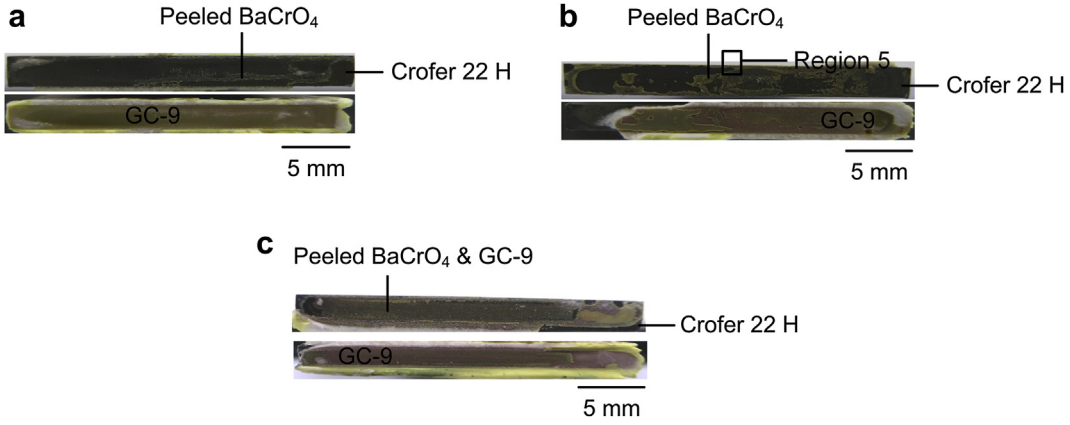

Fig. 8. Failure patterns in the tensile joint specimens: (a) short creep rupture time; (b) medium creep rupture time; (c) long creep rupture time.

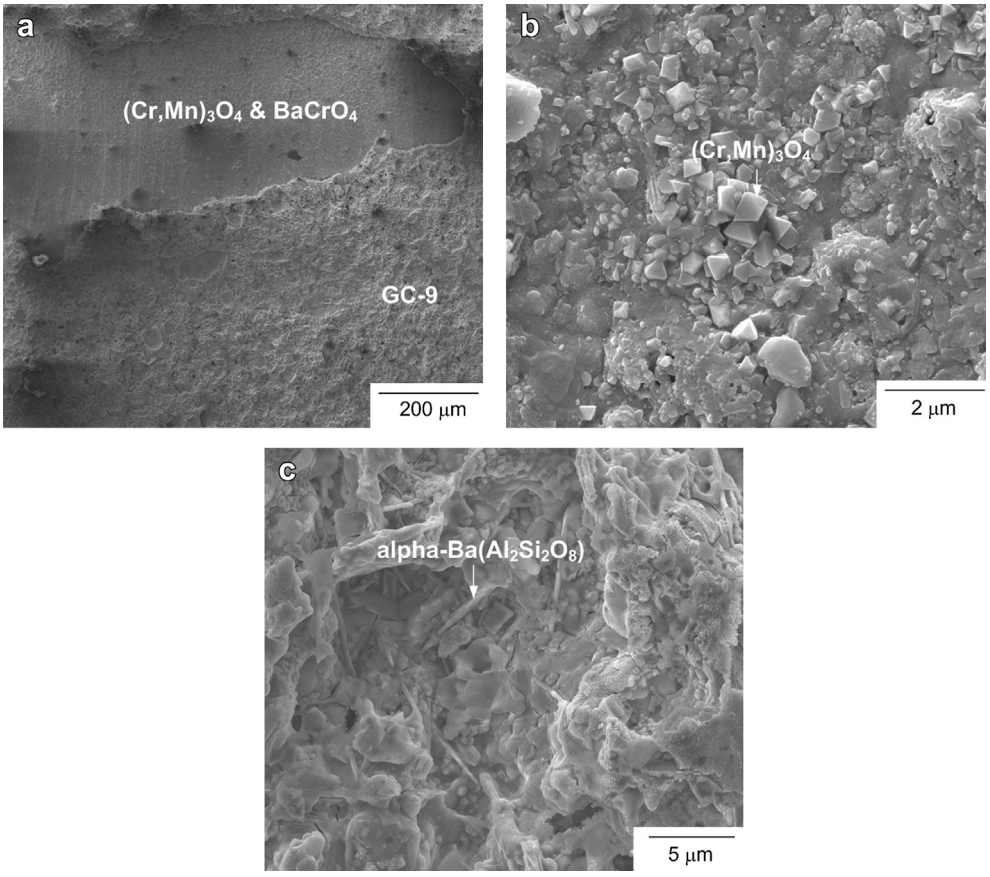

Fig. 9. (a) SEM micrograph of Region 5 in the tensile joint specimen of Fig. 8(b); (b) microstructure of the spinels buried in the chromate layer; (c) microstructure of the glass–ceramic substrate with residual chromate.

more brittle due to an in-situ crystallization mechanism during a creep test.

In summary, for both shear and tensile loading modes, cracking in the crept joint specimens initiates and grows at the spinel/chromate interface along the periphery of the joining area. The creep crack then penetrates through the chromate layer and propagates along the interface between the chromate layer and glass–ceramic substrate. Final fast fracture occasionally takes place within the glass–ceramic layer. For a longer creep rupture time, more crystalline phases are found in the glass–ceramic layer due to an in-situ crystallization mechanism. The yellow, pink, red, and brown regions observed on the fracture surface indicate a leftover chromate on top of the glass–ceramic substrate at different stages of the creep test. A dark color region such as red and brown is present in a specimen with a longer creep rupture time.

4. Conclusions

(1) For creep test of the Crofer 22 H/GC-9/Crofer 22 H joint specimens at 800 °C, the creep rupture time is shorter than 10 h when the applied stress is about 1.6 MPa and above in both shear and tensile loading modes. If the applied stress is less than 1.1 MPa, the creep rupture time is over 1000 h for both loading modes. The shear creep strength at 1000 h is about 23% of the average shear joint strength at 800 °C. The tensile creep strength at 1000 h is only about 9% of the average tensile joint strength at 800 °C.

(2) For both shear and tensile joint specimens, creep cracking first takes place at the spinel/$BaCrO_4$ interface, followed by penetration through the $BaCrO_4$ layer and propagation along the interface between the chromate layer and glass–ceramic substrate. Final fast fracture occasionally takes place within the glass–ceramic layer.

(3) An exhibition of various color regions on the fracture surface is attributable to the presence of leftover chromate. When the chromate layer is left on the Crofer 22 H side, a lime green color is observed. When the chromate is left on top of the glass–ceramic substrate, yellow, pink, red, and brown colors are observed at different stages of the creep test. A dark color region such as red and brown is present in a specimen with a longer creep rupture time.

Acknowledgments

This work was supported by the National Science Council (Taiwan) under Contract No. NSC 102-2221-E-008-018 and by the Institute of Nuclear Energy Research (Taiwan) under Contract No. 101-2001-INER-036.

References

[1] R. Bove, S. Ubertini, Modeling Solid Oxide Fuel Cells Methods, Procedures and Techniques, first ed., Springer, New York, 2008.
[2] P.A. Lessing, J. Mater. Sci. 42 (2007) 3465–3476.
[3] C.-K. Lin, T.-T. Chen, Y.-P. Chyou, L.-K. Chiang, J. Power Sources 164 (2007) 238–251.
[4] C.-K. Lin, L.-H. Huang, L.-K. Chiang, Y.-P. Chyou, J. Power Sources 192 (2009) 515–524.
[5] L. Blum, S.M. Gross, J. Malzbender, U. Pabst, M. Peksen, R. Peters, I.V. Vinke, J. Power Sources 196 (2011) 7175–7181.

[6] E.V. Stephens, J.S. Vetrano, B.J. Koeppel, Y. Chou, X. Sun, M.A. Khaleel, J. Power Sources 193 (2009) 625–631.
[7] J. Milhans, D.S. Li, M. Khaleel, X. Sun, M.S. Al-Haik, A. Harris, H. Garmestani, J. Power Sources 196 (2011) 5599–5603.
[8] J. Milhans, M. Khaleel, X. Sun, M. Tehrani, M. Al-Haik, H. Garmestani, J. Power Sources 195 (2010) 3631–3635.
[9] C.-K. Lin, K.-L. Lin, J.-H. Yeh, W.-H. Shiu, C.-K. Liu, R.-Y. Lee, J. Power Sources 241 (2013) 12–19.
[10] Y.-T. Chiu, C.-K. Lin, J.-C. Wu, J. Power Sources 196 (2011) 2005–2012.
[11] Y.-T. Chiu, C.-K. Lin, J. Power Sources 198 (2012) 149–157.
[12] J. Froitzheim, G.H. Meier, L. Niewolak, P.J. Ennis, H. Hattendorf, L. Singheiser, W.J. Quadakkers, J. Power Sources 178 (2008) 163–173.
[13] B. Kuhn, C.A. Jimenez, L. Niewolak, T. Hüttel, T. Beck, H. Hattendorf, L. Singheiser, W.J. Quadakkers, Mater. Sci. Eng. A 528 (2011) 5888–5899.
[14] F. Smeacetto, M. Salvo, M. Ferraris, V. Casalegno, P. Asinari, A. Chrysanthou, J. Eur. Ceram. Soc. 28 (2008) 2521–2527.
[15] Y.-S. Chou, J.W. Stevenson, P. Singh, J. Power Sources 184 (2008) 238–244.
[16] Y.-S. Chou, J.W. Stevenson, P. Singh, J. Power Sources 185 (2008) 1001–1008.
[17] J. Malzbender, Y. Zhao, J. Mater. Sci. 47 (2012) 4342–4347.
[18] J. Malzbender, Y. Zhao, Fuel Cells 12 (2012) 47–53.
[19] C.-K. Lin, J.-Y. Chen, J.-W. Tian, L.-K. Chiang, S.-H. Wu, J. Power Sources 205 (2012) 307–317.
[20] H.-T. Chang, C.-K. Lin, C.-K. Liu, S.-H. Wu, J. Power Sources 196 (2011) 3583–3591.
[21] H.-T. Chang, C.-K. Lin, C.-K. Liu, J. Power Sources 195 (2010) 3159–3165.
[22] H.-T. Chang, C.-K. Lin, C.-K. Liu, J. Power Sources 189 (2009) 1093–1099.
[23] Y.-T. Chiu, C.-K. Lin, J. Power Sources 219 (2012) 112–119.
[24] C.-K. Liu, T.-Y. Yung, K.-F. Lin, R.-Y. Lee, T.-S. Lee, Glass-Ceramic Sealant for Planar Solid Oxide Fuel Cells, United States Patent No. 7,897,530 B2, 2011.
[25] C.-K. Liu, T.-Y. Yung, K.-F. Lin, in: Proceedings of the Annual Conference of the Chinese Ceramic Society 2007 (CD-ROM), 2007 (in Chinese).
[26] C.-K. Liu, T.-Y. Yung, S.-H. Wu, K.-F. Lin, in: Proceedings of the MRS_Taiwan Annual Meeting 2007 (CD-ROM), 2007 (in Chinese).
[27] C.-K. Liu, T.-Y. Yung, K.-F. Lin, in: Proceedings of the Annual Conference of the Chinese Ceramic Society 2008 (CD-ROM), 2008 (in Chinese).
[28] C.-K. Liu, K.-C. Tsai, K.-F. Lin, S.-H. Wu, T.-Y. Yung, in: Proceedings of the Annual Conference of the Chinese Ceramic Society 2009 (CD-ROM), 2009 (in Chinese).
[29] C.-K. Liu, T.-Y. Yung, K.-F. Lin, R.-Y. Lee, S.-H. Wu, ECS Trans. 25 (2009) 1491–1500.
[30] I.W. Donald, J. Mater. Sci. 28 (1993) 2841–2886.